electronics

MDPI

Article

A Variable-Weather-Parameter Optimization Strategy Based on an Irradiance and Temperature Estimation Method for PV System

Shaowu Li

College of Intelligent Systems Science and Engineering, Hubei Minzu University, Enshi 445000, China; xidu_surfer@163.com; Tel.: +86-139-9779-9701

Abstract: The variable-weather-parameter (VWP) methods have the fastest maximum power point tracking (MPPT) speed because their control signals are directly calculated by the measured weather data (including irradiance and temperature (I&T) data). However, they are suffering from the high hardware cost of the I&T sensors. To solve this problem, an estimation method to estimate the real-time I&T values is proposed. In this method, an equation set and two empirical equations are established to match the changeless and varying weather conditions, respectively. Based on them, a VWP optimization strategy (VWPOS) is proposed. It is without using I&T sensors (or external I&T data) that the advantage of the MPPT rapidity is inherited from the VWP methods. Finally, some simulation experiments involving the VWPOS are conducted, and the results show that the estimation method is accurate and workable regardless of the changeless or varying weather conditions. Meanwhile, simulation results also show that the tracking speed of an existing MPPT method can be greatly optimized by the VWPOS even if the I&T sensors or external I&T data are not used. In addition, simulation results still show that, when the conventional P&O method is optimized by the VWPOS, the average error of its control signal at the MPP can be decreased from 0.025% to 0.005%, and the settling time of its output power can be decreased to at least one-third of the original value. With this work, for the existing VWP methods, the trouble arising from the hardware cost of the I&T sensors can be prevented, which is beneficial to their widespread use.

Keywords: PV system; MPPT; estimation method; optimization strategy; MPP

Citation: Li, S. A Variable-Weather-Parameter Optimization Strategy Based on an Irradiance and Temperature Estimation Method for PV System. *Electronics* **2022**, *11*, 1439. https://doi.org/10.3390/electronics11091439

Academic Editor: Olivier Sename

Received: 13 March 2022
Accepted: 22 April 2022
Published: 29 April 2022

1. Introduction

Up to now, lots of the MPPT methods are presented [1–4]. In them, the I&T sensors are involved in some designs to achieve good MPPT performance. For example, two VWP methods are first proposed to obtain the fastest MPPT speed and simpler control process [5]. Meanwhile, to increase the seeking speed and adaptability, a VWP method based on input resistance is also proposed [6]. In addition, a VWP method is proposed to simplify the control complexity and guarantee a good MPPT speed when the inverter is involved in the MPPT control [7]. The main advantages of these presented VWP methods are the good MPPT speed, simple control process, and strong adaptability to the fast-varying weather or load. However, the I&T sensors must be used for them, which implies a higher hardware cost. In order to solve this problem, in this paper, a VWPOS without I&T sensors is proposed. Unlike the existing VWP methods, in this strategy, the I&T sensors are abandoned, and only some expressions are used to calculate the real-time values of the irradiance and temperature. Clearly, for these existing VWP methods, which are suffering from the hardware cost of the I&T sensors, this work sweeps away the key obstacle to their widespread use.

Certainly, some attempts have been made in some MPPT algorithms to abandon the irradiance or temperature sensors. For example, to improve the MPPT performance of the conventional P&O method, a short-circuit current method with an irradiance sensorless

control is presented [8]. However, in this work, because the real-time value of the short-circuit current needs to be measured, the MPPT performance and system complexity are greatly influenced. In addition, to reduce the hardware cost arising from I&T sensors, a VWP method based on weather forecast data is proposed [9]. However, in this work, the real-time external data of the weather forecast must be obtained to estimate the control signal, which implies that extra equipment must be used to obtain these data. Meanwhile, the MPPT performance is greatly influenced by the accuracy of the weather forecast data. Clearly, in these works, some serious shortcomings appeared after the I&T sensors were thrown away. In order to deal with this difficult problem, in this paper, an I&T estimation method is proposed, and three equations (including an equation set and two empirical equations) are presented. By using these three equations, the real-time values of the irradiance and temperature can be successfully estimated only by the measured data of the output voltage and current. In this case, the real-time control signal can be approximately calculated. On the basis of this estimated control signal, the proposed VWPOS is designed to implement tracking speed optimization without using I&T sensors or external I&T data. Obviously, no extra sensor or external data reveal the lower hardware cost and better control independence.

Nowadays, some hybrid MPPT methods are designed to achieve two or more different performances, such as tracking speed, tracking accuracy, tracking overshoot, tracking efficiency, steady-state oscillation, hardware cost, control complexity, and so on. For example, the INC method is combined with the shuffled frog-leaping and pattern search algorithm to reduce the fuzzy rules and cost [10]. The P&O method is combined with the sliding-mode control to improve the robustness and tracking accuracy [11]. The P&O method and PSO method are combined to harvest a good tracking speed and zero oscillation [12]. The three-point weight method is united with the FLC method to decrease the system complexity and MPPT efficiency [13]. The FLC method and PSO method are combined to obtain the MPP under varying weather [14]. In these works, the various combination points are designed to simultaneously obtain as many good performances as possible. In this proposed VWPOS, the characteristics between irradiance, temperature, load, and control signal at the MPP are first used as the switching point to combine the VWP method with the P&O method. By this design, complementary advantages can be achieved. Here, the advantages, including the good tracking speed, simple control algorithm, and strong adaptability, originate from the VWP method, while the zero overshoot and easy implementation arise from the P&O method. Clearly, this design is very different from all existing MPPT hybrid methods.

Hitherto, lots of work has been performed to study the P&O method, which is one of the widest used MPPT schemes [15,16]. For example, to decrease the response time and power losses, two improved P&O methods are presented [17,18]. Meanwhile, to avoid the drift effect arising from the fast-changing weather, the P&O method is improved by incorporating the current information [19]. In addition, an improved P&O method is proposed to guarantee tracking accuracy [20]. Although so many efforts have been made to improve the various MPPT performances of the P&O method, the contradiction between MPPT speed and tracking step size is still not solved well. In order to reconcile this contradiction, in this manuscript, the conventional P&O method is selected as the object optimized by the VWPOS. By using the VWPOS, the speed to search the MPP can hardly be influenced by the different seeking step sizes. Clearly, it is extremely beneficial to achieve good steady-state performance by decreasing the tracking step size because the smaller step size implies better steady-state accuracy and oscillation.

The main aims, innovations, and contributions of this work can be illustrated as follows:

(1) An equation set for estimating the real-time I&T values under changeless weather conditions is established. This work is the first attempt to obtain the real-time I&T values by equation solution at the MPP of the PV system.
(2) Two equations for estimating the real-time irradiance values under varying weather conditions are proposed. This work is the first attempt to estimate the real-time irradiance by two established empirical formulas.

(3) A VWP optimization strategy based on the estimated I&T values is proposed, and its control process is designed. This work is the first attempt to implement the VWP method by estimating the real-time values of the irradiance and temperature.
(4) In this work, the external data or measured values of the irradiance and temperature are no longer needed to implement the existing VWP methods. Therefore, it is a major breakthrough in cutting the cost of sensors and promoting the use of these methods.

This paper is arranged as follows: the I&T estimation method under changeless weather conditions is presented in Section 2, while this method under varying weather conditions is analyzed in Section 3. The VWPOS based on the I&T estimation method is proposed, and the control process is designed in Section 4. The accuracy and workability of the I&T estimation method are verified, the feasibility and availability of the VWPOS are tested, and the MPPT optimization effect of the VWPOS is analyzed in Section 5. Some discussions are given in Section 6. Finally, there are some conclusions drawn in Section 7.

2. Estimation Method under Changeless Weather Conditions

2.1. Mathematical Model of PV System

Figure 1 shows the usual configuration of the PV system. The mathematical models of the PV cell [21,22], buck DC/DC converter [23], and load can be expressed by Equation (1), Equation (2), and Equation (3), respectively. Here, other DC/DC converters can also be used, and the results can be analyzed by analogy. In addition, the load may be a DC bus, an inverter, or batteries. In this case, an equivalent load can still be used to represent them.

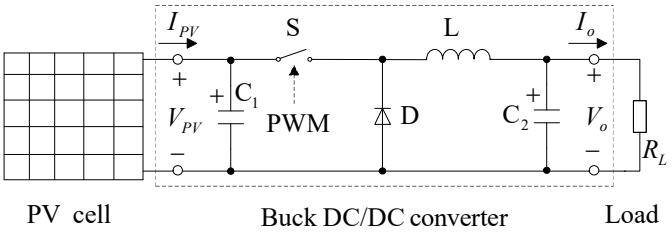

Figure 1. Configuration of the usual PV system.

$$I_{PV} = I_{sc}[1 - C_1(e^{\frac{V_{PV}}{C_2 V_{oc}}} - 1)] \quad (1)$$

$$V_o = DV_{PV} \quad (2)$$

$$P_o = V_o^2 / R_L = V_o I_o \quad (3)$$

where $C_1 = (1 - I_m/I_{sc})\exp(-V_m/C_2V_{oc})$; $C_2 = (V_m/V_{oc} - 1)/\ln(1 - I_m/I_{sc})$. V_m, I_m, V_{oc} and I_{sc} represent the MPP voltage, the MPP current, the open-circuit voltage, and the short circuit current, respectively. D represents the duty cycle of the PWM signal of the DC/DC converter. Their initial values are usually given by the PV array manufacturer at standard test conditions (STC).

$$P_o = \frac{R_L I_{sc}^2}{D^2}[1 - C_1(e^{\frac{\sqrt{P_o R_L}}{C_2 V_{oc} D}} - 1)]^2 \quad (4)$$

If the converter and load are assumed as the ideal circuits or elements, Equation (4) can be given by Equations (1)–(3). It is the theoretical model of the PV system corresponding to Figure 1 [5].

The relationship between P_o and D shown in Equation (4) is the theoretical basis for designing the I&T estimation method and then proposing the MPPT optimization strategy.

2.2. Principle of the Parameter Estimation

According to my previous work in Refs. [5,6], an equation set (Equation (5)) is satisfied when the PV system is operating at the MPP. Where $V_{PV}|_{\mathrm{MPP}}$ and $P_o|_{\mathrm{MPP}}$ represent the output voltage of the PV cell and output power of the PV system, respectively, when the

PV system is operating at the MPP. S and T represent the real-time values of the irradiance and temperature. Clearly, according to Equation (5), if the real-time values of $V_{PV}|_{\mathrm{MPP}}$ and $P_o|_{\mathrm{MPP}}$ can be measured, S and T can be solved by the equation solution.

$$\begin{cases} V_{PV}|_{\mathrm{MPP}} = C(S,T) \\ P_o|_{\mathrm{MPP}} = P_o(S,T) \end{cases} \tag{5}$$

According to Equation (2), Equation (6) is satisfied. Here, $D_{\max}$ and $V_{o\max}$ represents the duty cycle and output voltage, respectively, when the PV system is operating at the MPP.

$$V_{PV}|_{\mathrm{MPP}} = \frac{V_{o\max}}{D_{\max}} \tag{6}$$

According to Equation (3), Equation (7) is satisfied. Here, $I_{o\max}$ represents the output current when the PV system is operating at the MPP.

$$P_o|_{\mathrm{MPP}} = V_{o\max} I_{o\max} \tag{7}$$

The real-time values of $V_{o\max}$ and $I_{o\max}$ can be obtained by sampling V_o and I_o when the PV system is just operating at its MPP. According to Equations (6) and (7), an equation set can be established and shown in Equation (8). Where S_m and T_m represent the equation solutions of S and T, respectively, corresponding to the MPP.

$$\begin{cases} P_o(S_m, T_m) = V_{o\max} I_{o\max} \\ C(S_m, T_m) = V_{o\max}/D_{\max} \end{cases} \tag{8}$$

In practical application, $D_{\max}$ can be directly read by the controller, so the real-time value of S_m and T_m can be solved by Equation (8) after $V_{o\max}$ and $I_{o\max}$ have been measured successfully.

Therefore, when the weather conditions keep unchanged, the irradiance and temperature can be calculated in real time. If the sampled values of $V_{o\max}$ and $I_{o\max}$ are accurate enough, the estimated values of the irradiance and temperature will be very accurate.

3. Estimation Method under Varying Weather Conditions

3.1. MPP Characteristics Changing with Weather Conditions

In practical application, the weather conditions are usually changeable. In other words, the irradiance and temperature usually keep varying. Therefore, in this work, the question of how to quickly estimate the irradiance and temperature under varying weather conditions must be studied.

In order to analyze this issue, some simulation experiments are performed to study the characteristics between parameters (including irradiance, temperature, and load) and control signal at the MPP. These simulations are finished under ideal conditions, and the results are shown by some $P_o - D$ curves in Figures 2–4. Here, the four cell parameters I_{sc}, V_{oc}, I_m, and V_m are selected as 9.19 A, 22 V, 8.58 A and 17.5 V at STC, respectively. Figure 2 shows the $P_o - D$ curves under different irradiance, 20 °C and 0.5 Ω conditions. The $P_o - D$ curves under different temperatures, 800 W/m^2 and 0.5 Ω conditions, are shown in Figure 3. The $P_o - D$ curves under different load, 800 W/m^2 and 20 °C conditions are shown in Figure 4.

According to Figures 2–4, it can be seen that, firstly, the control signal at the MPP (represented by $D_{\max}$) will move to the right when the irradiance, temperature, or load keeps increasing. Secondly, the output power at the MPP (represented by $P_{o\max}$) will increase, decrease and keep constant with the increase in S, T and R_L, respectively. Thirdly, the influence of the irradiance to $P_{o\max}$ is far greater than that of the temperature or load.

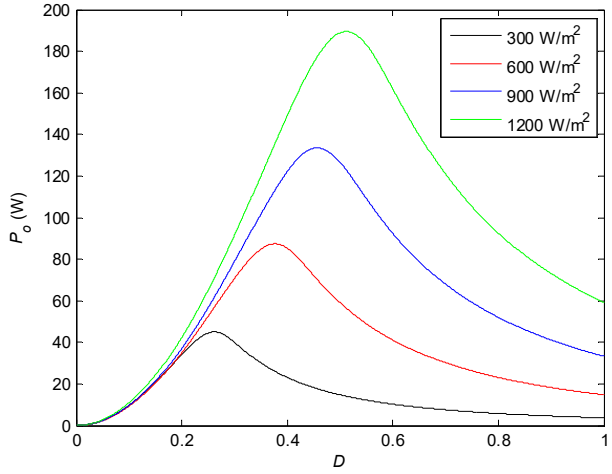

Figure 2. Curves under different irradiance conditions.

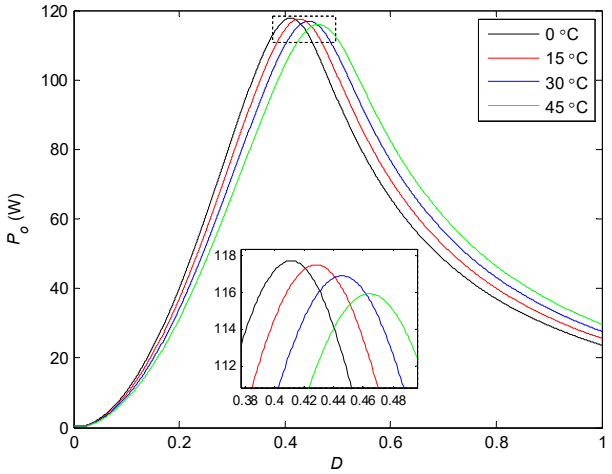

Figure 3. $P_o - D$ curves under different temperature conditions.

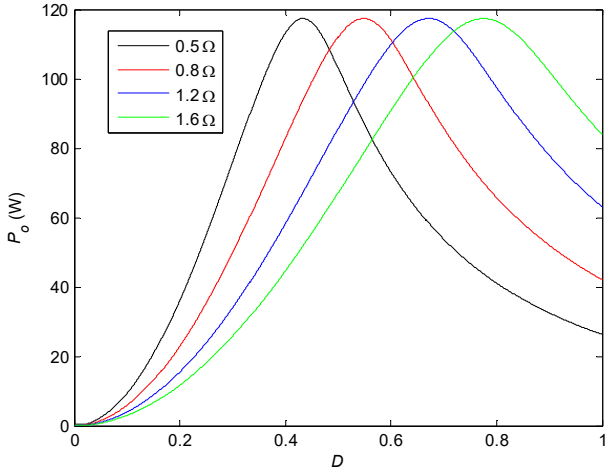

Figure 4. Curves under different load conditions.

In order to further verify these results shown in Figures 2–4, some simulation experiments have been performed under ideal conditions, and the results are shown in Tables 1–3.

Table 1. MPP values under different irradiance, 20 °C and 1 Ω conditions.

S (W/m^2)	200	300	400	500	600	700	800	900	1000	1100	1200
$P_{o\max}$ (W)	30.65	44.90	59.04	73.15	87.33	102.02	117.27	133.47	150.83	169.45	189.48
$D_{\max}$	0.3001	0.3705	0.4314	0.4852	0.5327	0.5754	0.6131	0.6466	0.6761	0.7018	0.7239

Table 2. MPP values under different temperature, 800 W/m^2 and 1 Ω conditions.

T (°C)	0	5	10	15	20	25	30	35	40	45	50
$P_{o\max}$ (W)	117.74	117.54	117.62	117.47	117.27	117.16	116.73	116.63	116.21	115.91	115.48
$D_{\max}$	0.5813	0.5887	0.5971	0.6050	0.6131	0.6216	0.6295	0.6386	0.6470	0.6561	0.6650

Table 3. MPP values under different load, 800 W/m^2 and 20 °C conditions.

R_L (Ω)	0.4	0.6	0.8	1.0	1.2	1.4	1.6	1.8	2.0
$P_{o\max}$ (W)	117.06	117.28	117.18	117.27	117.25	117.32	117.34	117.35	117.31
$D_{\max}$	0.3874	0.4749	0.5481	0.6131	0.6716	0.7256	0.7757	0.8228	0.8672

Table 1 shows that when only the irradiance varies from 200 W/m^2 to 1200 W/m^2, $D_{\max}$ will increase and change from 0.3001 to 0.7239, and $P_{o\max}$ will also increase and change from 30.65 W to 189.48 W. Table 2 shows that when only the temperature varies from 0 °C to 50 °C, $D_{\max}$ increases while $P_{o\max}$ decreases. Meanwhile, in all simulation data of $D_{\max}$ and $P_{o\max}$, the biggest values of the error are 0.0837 and 2.26 W, respectively. Table 3 shows that when only the load varies from 0.4 Ω to 2.0 Ω, $P_{o\max}$ it approximately keeps constant, while $D_{\max}$ increases from 0.3874 to 0.8672.

Therefore, some conclusions can be given: on the one hand, $D_{\max}$ is greatly influenced by the varying irradiance and load, while it is hardly influenced by the varying temperature. On the other hand, $P_{o\max}$ is greatly influenced by the varying irradiance, while it is hardly influenced by the varying temperature and load. These conclusions can be used to estimate the real-time I&T values. Meanwhile, they are also used to design the MPPT optimization method without I&T sensors.

3.2. Proposed Equations for Estimating the Real-Time Irradiance

Equation (8) clearly shows that the real-time I&T values can be calculated after the PV system reaches its MPP under varying weather conditions. Based on these calculated values, in Figure 5, when the changing weather conditions lead to the MPP moving from point A to point B, the irradiance corresponding to point A must be calculated to estimate the approximate value of $D_{\max 2}$. Therefore, two groups of simulation experiments are performed to obtain the value of the irradiance corresponding to point B. Here, S_m and T_m represent the irradiance and temperature values calculated by Equation (8), respectively, at the point A. P_{om} represents the maximum power at the point A. Its value can be calculated by Equation (9) after $V_{o\max}$ and $I_{o\max}$ at the point A have been measured.

$$P_{om} = V_{o\max} I_{o\max} \tag{9}$$

On the one hand, a group of simulations are conducted under increasing irradiance conditions. Figure 5 shows the $P_o - D$ curves, and Table 4 shows the simulation results. In Figure 5, the point A (P_{om}, S_m, T_m) and point B (P_{omI}, S_I, T_I) represent the MPP before and after the irradiance changes, respectively.

According to Table 4, Equation (10) can be presented to show the relationship between S_I and S_m when the irradiance keeps increasing. In Equation (10), P_o represents the power corresponding to the control signal $D_{\max 1}$ after the irradiance has increased. Clearly, the operating point C (P_o, S_I, T_I) is not the MPP when the duty cycle of the converter is equal to $D_{\max 1}$. Namely, there is a mismatch between the control signal and weather conditions

in this case. The value of P_o can be measured if the PV system is operating at point A while the irradiance has changed from A to B.

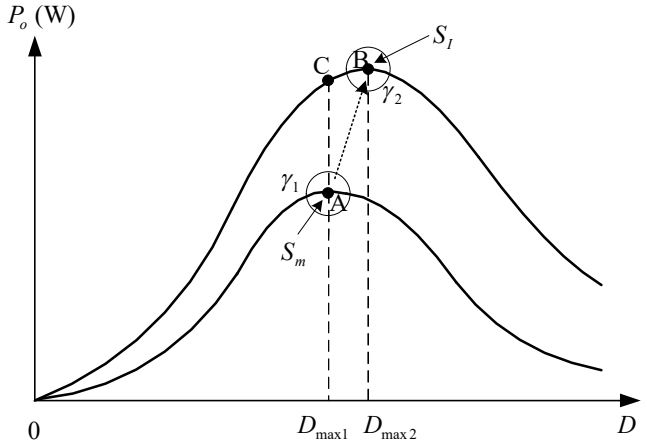

Figure 5. Characteristics of the MPP moving with the increasing irradiance.

Table 4. Simulation results under increasing irradiance conditions.

S_I (W/m^2)		400	500	600	700	800	900	1000	1100	1200
S_m = 300 (W/m^2)	P_o (W)	52.96	55.60	57.02	58.31	59.85	61.83	64.34	67.44	71.15
S_m = 400 (W/m^2)	P_o (W)	/	68.22	72.45	75.34	78.08	81.16	84.81	89.16	94.28
S_m = 500 (W/m^2)	P_o (W)	/	/	83.40	89.38	94.08	98.69	103.74	109.50	116.11
S_m = 600 (W/m^2)	P_o (W)	/	/	/	98.74	106.60	113.38	120.19	127.56	135.78
S_m = 700 (W/m^2)	P_o (W)	/	/	/	/	114.67	124.57	133.68	142.97	152.96
S_m = 800 (W/m^2)	P_o (W)	/	/	/	/	/	131.36	143.39	154.96	166.92
S_m = 900 (W/m^2)	P_o (W)	/	/	/	/	/	/	149.09	163.34	177.49
S_m = 1000 (W/m^2)	P_o (W)	/	/	/	/	/	/	/	168.06	184.59

$$S_I = \frac{100(P_o - P_{om}) - 446 - 1.2S_m}{0.018S_m - 3.6} + S_m + 100 \quad (10)$$

On the other hand, a group of simulations are conducted under decreasing irradiance conditions. Figure 6 shows the $P_o - D$ curves, and Table 5 shows the simulation results. In Figure 6, the point A (P_{om}, S_m, T_m) and point B (P_{omD}, S_D, T_D) represent the MPP before and after the irradiance changes, respectively.

Table 5. Simulation results under decreasing irradiance conditions.

S_D (W/m^2)		900	800	700	600	500	400	300
S_m = 1000 (W/m^2)	P_o (W)	131.81	110.09	86.81	64.52	44.97	28.81	16.21
S_m = 900 (W/m^2)	P_o (W)	/	115.17	93.28	70.20	49.12	31.50	17.73
S_m = 800 (W/m^2)	P_o (W)	/	/	99.325	77.05	54.47	35.01	19.71
S_m = 700 (W/m^2)	P_o (W)	/	/	/	84.01	61.30	39.70	22.38
S_m = 600 (W/m^2)	P_o (W)	/	/	/	/	69.05	46.08	26.09
S_m = 500 (W/m^2)	P_o (W)	/	/	/	/	/	54.09	31.38

According to Table 5, Equation (11) can be presented to show the relationship between S_D and S_m when the irradiance keeps decreasing. In Equation (11), P_o represents the power corresponding to the control signal D_{max1} after the irradiance has decreased. Its value can also be measured if the PV system is operating at point A while the irradiance has changed from A to B. Meanwhile, the operating point C (P_o, S_D, T_D) is not the MPP when the duty cycle of the converter is equal to D_{max1}. Namely, there is also a mismatch between the control signal and weather conditions in this case.

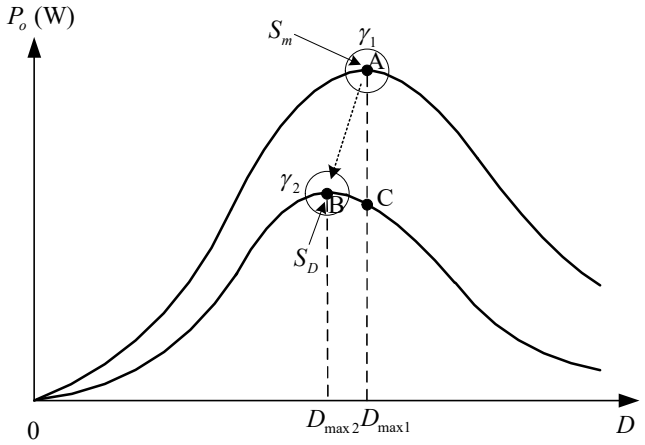

Figure 6. Characteristics of the MPP moving with the decreasing irradiance.

$$S_D = \frac{50(P_o - P_{om} + 18.1)}{11} + S_m - 100 \tag{11}$$

Therefore, when the weather conditions keep varying, Equations (10) and (11) can be used to estimate the real-time value of the irradiance.

3.3. Estimation of the Real-Time Temperature

In practical application, the temperature can usually be regarded as a constant. The reasons can be illustrated as follows: firstly, the temperature usually keeps unchanged within a short time. Secondly, according to Figure 3 and Table 2, $P_{o\max}$ is hardly influenced by the varying temperature. Therefore, Equations (12) and (13) are used to approximately estimate the real-time value of the temperature.

$$T_I = T_m \tag{12}$$

$$T_D = T_m \tag{13}$$

All in all, according to Equations (8) and (10)–(13), the real-time I&T values can be estimated. However, in practical application, there maybe exist some errors in the parameter estimation. Therefore, two regions, γ_1 and γ_2 (shown in Figures 5 and 6), can be used to replace the points A and B, respectively. In this case, two regions γ_1 and γ_2, actually reflect the error range of the estimated irradiance and temperature. Here, on the one hand, the reasonable regions γ_1 and γ_2 should be selected to consider all errors arising from all estimations of Equations (8) and (10)–(13). On the other hand, the question arising from the mismatch between the control signal and weather condition can be solved well by Equations (10) and (11) under varying weather conditions.

4. MPPT Optimization Strategy

4.1. Principle and Description

After two reasonable regions, γ_1 and γ_2, have been obtained by the real-time I&T estimation, a new MPPT optimization strategy can be designed under varying weather conditions. This optimization strategy can be described as follows: when an existing MPPT method is selected to seek the MPP, because of the changing R_L, S or T conditions, the MPP will move from point A to point B (shown in Figures 7–9). In this moving process, the control signal can be first restricted to a small region γ_2, and then the MPP is tracked by this selected MPPT method within γ_2. By analogy, this optimization strategy is still feasible and available when the MPP moves from point B to point A.

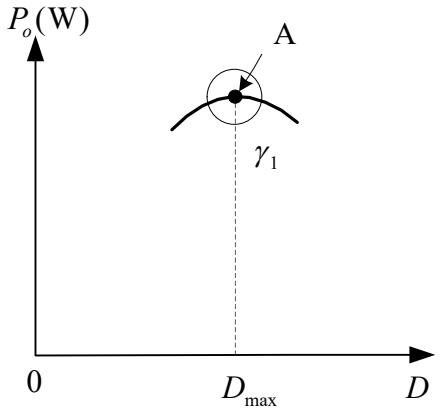

Figure 7. Regularity under (1) or (3) conditions.

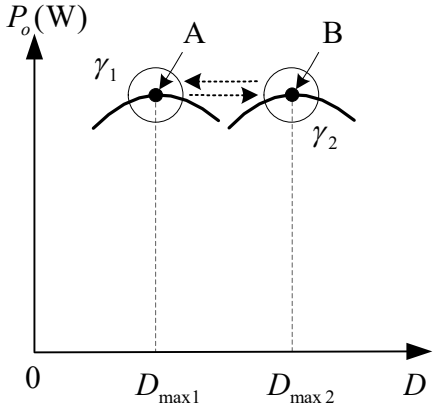

Figure 8. Regularity under (4) or (6) conditions.

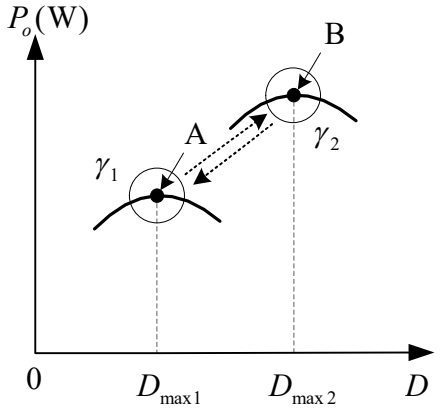

Figure 9. Regularity under (2), (5), (7) or (8) conditions.

Table 6. Eight operating conditions of PV system.

Operating Conditions	(1)	(2)	(3)	(4)	(5)	(6)	(7)	(8)
S (W/m^2)	constant	varying	constant	constant	varying	constant	varying	varying
T (°C)	constant	constant	varying	constant	varying	varying	constant	varying
R_L (Ω)	constant	constant	constant	varying	constant	varying	varying	varying

In order to analyze the MPPT control process of this optimization strategy, eight cases are taken into account as the operating conditions of the PV system, and they are shown in Table 6.

According to the conclusions shown in Section 3.1, for these eight cases, (1) and (3) are almost the same, (4) and (6) are almost the same, (2), (5), (7) and (8) are almost the same. In order to propose the VWPOS, the regular patterns of the varying $P_{o\max}$ and $D_{\max}$ under (1) or (3) conditions, under (4) or (6) conditions and under (2), (5), (7) or (8) conditions can be illustrated in Figure 7, Figure 8, and Figure 9, respectively. Here, two small regions around the MPP (including γ_1 and γ_2) are defined and we assume that, when the irradiance, temperature, load, or their combination is varying, the actual MPP (A or B) can always be within them. Where A and B represent the maximum power points (MPPs) before and after the conditions change, respectively, γ_1 and γ_2 represent the defined regions corresponding to A and B, respectively.

According to Figure 7, under (1) and (3) conditions, the MPP of the PV system does hardly change, so this existing MPPT method need not be optimized. Under (4) and (6) conditions, according to Figure 8, the MPP keeps constant while the control signal corresponding to it ($D_{\max}$) will keep varying. Now the control signal is first forced to move from γ_1 to γ_2, and then this existing MPPT method without this optimization strategy is used to search for the new MPP within γ_2. Under (2), (5), (7) or (8) conditions, according to Figure 9, both the MPP and its corresponding control signal keep varying. Now the control signal is still first forced to move from γ_1 to γ_2, and then this existing MPPT method without this optimization strategy is used to search the new MPP within γ_2. In addition, if A and B represent the MPPs after and before the conditions change, respectively, the control process can be analyzed by analogy.

Obviously, when the MPP of the PV system is tracked by an existing MPPT method, its seeking time can be greatly saved because the seeking range has been contracted within γ_1 or γ_2. Because most existing MPPT methods have a control process to search the MPP, two defined regions (γ_1 and γ_2) can increase their seeking speed, which is the principle of the VWPOS to optimize the tracking speed of an existing MPPT method.

4.2. Implementation

In order to implement the proposed MPPT optimization strategy, on the one hand, the reasonable regions γ_1 and γ_2 should be obtained. In this work, a conclusion in my previous work Ref. [5] is used and shown by Equation (14). In practical application, by analogy, other conclusions can also be used to obtain the regions γ_1 and γ_2.

$$D_{\max} = \frac{\sqrt{P_{o\max} R_L}}{C} \tag{14}$$

When an existing MPPT method is optimized by this optimization strategy, the global MPPT process is converted into a local search because of the contracted seeking range. Therefore, by using this strategy, not only all merits of this selected existing MPPT method is inherited, but also the merits of the VWP method are achieved by using Equation (14). This MPPT optimization strategy can be named the VWPOS. Obviously, the complementary merits of the optimized MPPT method and VWP method can be harvested by the VWPOS.

In addition, the main advantage of the VWPOS is that the I&T sensors or external I&T data need not be used. By contrast, when the VWP methods are implemented, the I&T sensors must be used to measure the real-time weather data. Therefore, the hardware cost for sensors or other detecting circuits can be greatly reduced by using the VWPOS.

According to Section 4.1, the controller structure and flow chart for implementing the VWPOS can be shown in Figures 10 and 11, respectively. In Figure 10, V_o and I_o are measured by the voltage and current detecting circuits (or sensors), respectively. By these real-time data, the values of $V_{o\max}$ and $I_{o\max}$ can be directly obtained, and the values of P_o, P_{om}, R_L can be directly calculated. According to Figure 10, clearly, the VWPOS, as well as most existing MPPT methods, just needs two detecting circuits (or sensors), which illustrates that there is no extra hardware cost.

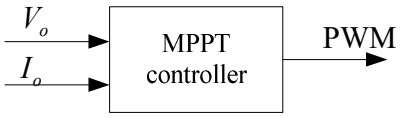

Figure 10. Controller structure of using the VWPOS.

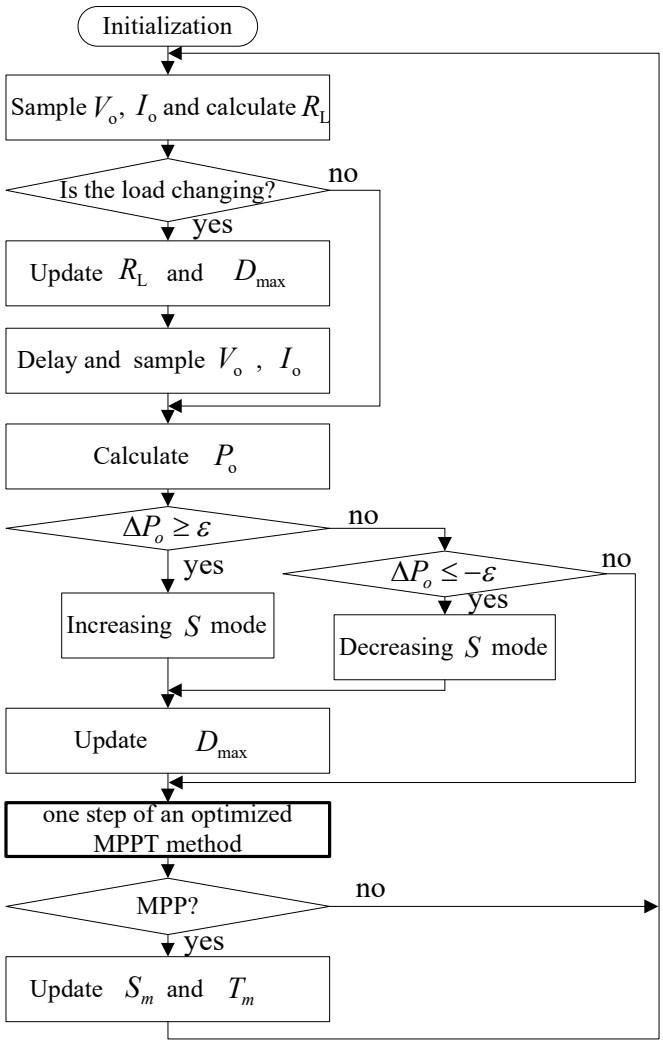

Figure 11. Flow chart of the VWPOS.

Before the PV system first arrives at its MPP, the MPP is searched only by the selected MPPT method. Namely, the seeking process can not be optimized. When the MPP is first arrived, S_m and T_m are calculated by Equation (8). These control tasks are finished in the step "Initialization". A control step of the optimized MPPT method is represented by the black bold box. In the step "Update R_L and $D_{\max}$", the value of $D_{\max}$ is calculated by Equation (14) when S and T are equal to S_m and T_m, respectively. Namely, Equation (15) is satisfied.

$$D_{\max} = \frac{\sqrt{P_{o\max}(S_m, T_m)R_L}}{C(S_m, T_m)} \tag{15}$$

In the steps "Increasing S mode" and "Decreasing S mode", S_I and S_D are calculated by Equation (10) and Equation(11), respectively. They can be used to calculate the value of $D_{\max}$ according to Equation (14) in the step "Update $D_{\max}$". If the "Increasing S mode"

step is available, Equation (16) is satisfied while Equation (17) should be used to match the "Decreasing S mode" step.

$$D_{\max} = \frac{\sqrt{P_{o\max}(S_I, T_m)R_L}}{C(S_I, T_m)} \tag{16}$$

$$D_{\max} = \frac{\sqrt{P_{o\max}(S_D, T_m)R_L}}{C(S_D, T_m)} \tag{17}$$

Finally, in the step "Update S_m and T_m", the values of S_m and T_m are recalculated and updated by the measured data at the MPP. In addition, ε is a small positive number and it represents the threshold value of the increment or decrement of the output power. Its initial value is given in the step "Initialization".

According to Figure 11, obviously, all existing MPPT methods which have the seeking process for the MPP can be selected as the optimized object to improve the whole MPPT speed. By comparing the VWPOS with these methods, there exists a small increase in computational complexity. On the one hand, some steps which compute R_L, P_o, S_I, S_D, S_m and T_m are added. On the other hand, some judgement steps are used. Finally, some steps to update and assign some parameters are needed. However, the control complexity arising from these added simple computation, judgment, and assignment steps can be ignored in practical application. In addition, by comparing the VWPOS with some MPPT methods which need the irradiance and temperature data, such as the existing VWP methods and so on, it has a lower hardware cost because of the removed irradiance and temperature sensors or extra data terminals.

5. Simulation Experiments

5.1. Estimation Method under Changeless Weather Conditions

Some simulation experiments are performed to analyze the estimation method under arbitrary changeless weather conditions. The results are shown in Table 7. In these simulation experiments, the four cell parameters are the same as in Section 3.1, and the load resistance is selected as 1.5 Ω. In Table 7, $D^*_{\max}$, $V^*_{o\max}$ and $I^*_{o\max}$ represent the measured (or read) values of the duty cycle, output voltage, and output current, respectively, when the PV system is operating at the MPP. In addition, ΔS_m and ΔT_m are defined by Equations (18) and (19) to analyze the accuracy of the estimation method.

$$\Delta S_m = S - S_m \tag{18}$$

$$\Delta T_m = T - T_m \tag{19}$$

Table 7 shows that, firstly, S_m and T_m can be calculated by Equation (8) under given weather conditions, which means the feasibility and effectiveness of the estimation method under changeless weather conditions. Secondly, S_m and T_m are always approximately equal to their respective real values, although there are some errors. The maximum error of S_m is less than 4 W/m^2, while that of T_m is less than 0.8 °C. Thirdly, the mean values of ΔS_m and ΔT_m are about 0.0905 W/m^2 and 0.1745 °C, respectively, which means the good accuracy of the estimation method under changeless weather conditions.

In a word, under changeless weather conditions, the estimation method is feasible, available, and workable to obtain the real-time I&T values, and its accuracy is very good.

5.2. Estimation Method under Varying Weather Conditions

5.2.1. Simulation under Decreasing Irradiance Conditions

Two simulation experiments are performed to analyze the estimation method under varying weather conditions. Assuming that, in the first simulation, the PV system is operating under decreasing irradiance conditions (shown in Figure 12) while the increasing irradiance conditions are considered in the second one. Meanwhile, assuming that the estimation method starts operating at 0.3 s in these two simulations. In addition, assuming that the values of T and R_L are 25 °C and 1 Ω, respectively. When the irradiance changes

in Figure 12, the simulation results can be shown in Figures 13–17. In this case, the controller must operate at the "Decreasing S mode" twice. Here, to analyze the accuracy of the estimation method under varying weather conditions, ΔS_D and ΔS_I are defined by Equation (20) and Equation (21), respectively.

$$\Delta S_D = S - S_D \tag{20}$$

$$\Delta S_I = S - S_I \tag{21}$$

Table 7. Simulation results under arbitrary changeless weather conditions.

Weather Conditions (W/m^2, °C)	$D^*_{\mathbf{max}}$	$V^*_{o\mathbf{max}}$ (V)	$I^*_{o\mathbf{max}}$ (A)	S_m (W/m^2)	T_m (°C)	ΔS_m (W/m^2)	ΔT_m (°C)
(300,10)	0.442	8.231	5.487	299.358	9.415	0.642	0.585
(300,20)	0.454	8.221	5.481	301.759	19.221	−1.759	0.779
(450,10)	0.547	9.974	6.649	450.821	9.679	−0.821	0.321
(450,20)	0.562	9.963	6.642	452.867	19.524	−2.867	0.476
(550,15)	0.616	10.981	7.320	551.548	15.233	−1.548	−0.233
(550,22)	0.628	10.970	7.313	552.600	22.156	−2.600	−0.156
(650,20)	0.679	11.916	7.944	651.019	19.855	−1.019	0.145
(650,28)	0.694	11.899	7.933	651.556	27.753	−1.556	0.247
(800,25)	0.761	13.256	8.838	799.550	24.899	0.450	0.101
(800,30)	0.772	13.243	8.829	799.466	29.906	0.534	0.094
(800,35)	0.783	13.226	8.817	799.018	34.785	0.982	0.215
(950,25)	0.822	14.585	9.723	948.904	24.719	1.096	0.281
(950,35)	0.844	14.552	9.701	947.757	34.455	2.243	0.545
(1050,30)	0.868	15.462	10.308	1048.866	29.899	1.134	0.101
(1050,40)	0.892	15.421	10.281	1046.768	39.917	3.232	0.083
(1180,35)	0.917	16.623	11.082	1178.958	35.051	1.042	−0.051
(1180,40)	0.931	16.600	11.066	1177.646	40.567	2.354	−0.567

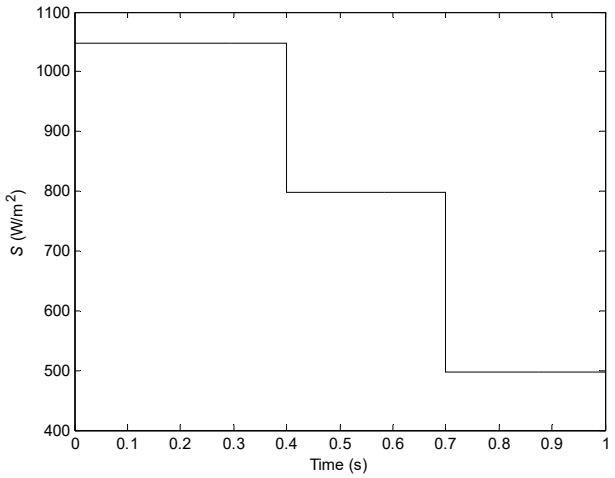

Figure 12. Assumed irradiance curve in first simulation.

Figures 13 and 14 show that, when the estimation method is used, S_m and I_m can be calculated by Equation (8) under decreasing irradiance conditions. Here, although there are some ripples that reveal the real-time errors between these two parameters and their calculated values, the mean values are approximately accurate. Figure 15 shows that S_D can be successfully calculated by Equation (11) when the irradiance keeps decreasing. Figure 16 shows that, firstly, S_m has a very small error under decreasing irradiance conditions. Secondly, there is a small error for S_D. Thirdly, when there is a sudden change in the irradiance, their errors exist in the peak values because of the inertia and delay of the whole

PV system. Figure 17 shows that, on the one hand, the mean values of T_m have a small error under decreasing irradiance conditions. On the other hand, there exists some oscillation for these errors because of the inertia and delay of the PV system, especially at the time of the sudden change of the irradiance.

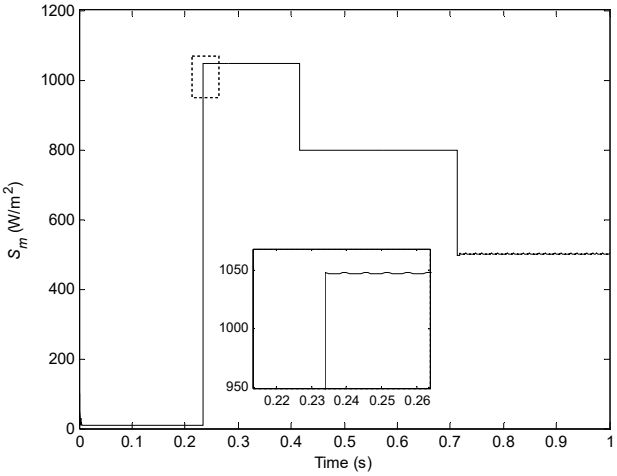

Figure 13. Curve in first simulation.

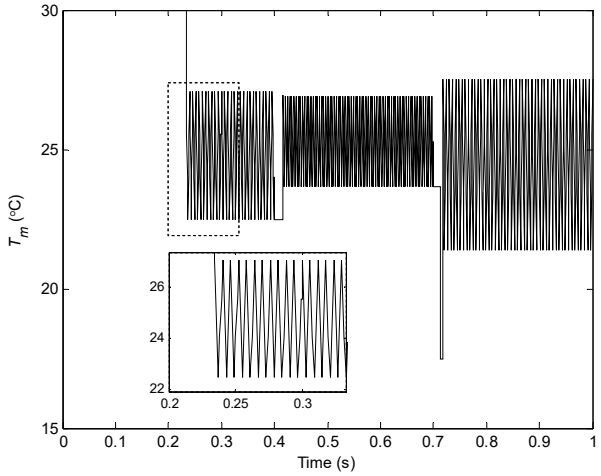

Figure 14. Curve in first simulation.

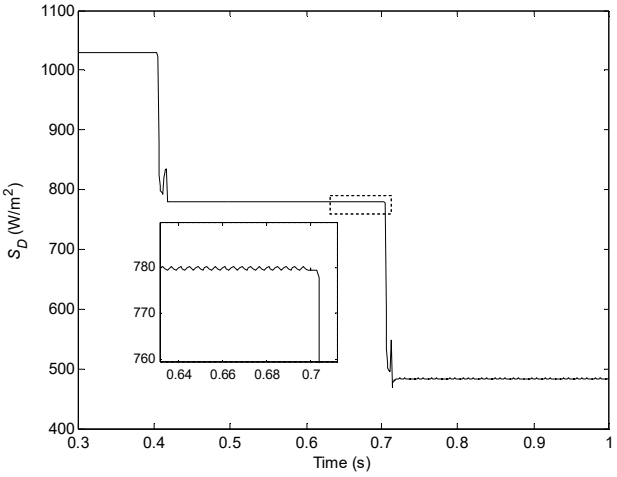

Figure 15. S_D curve in first simulation.

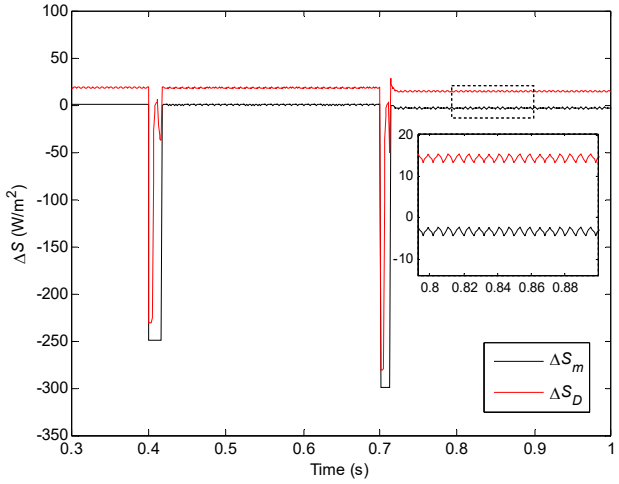

Figure 16. ΔS_D curves under decreasing S conditions.

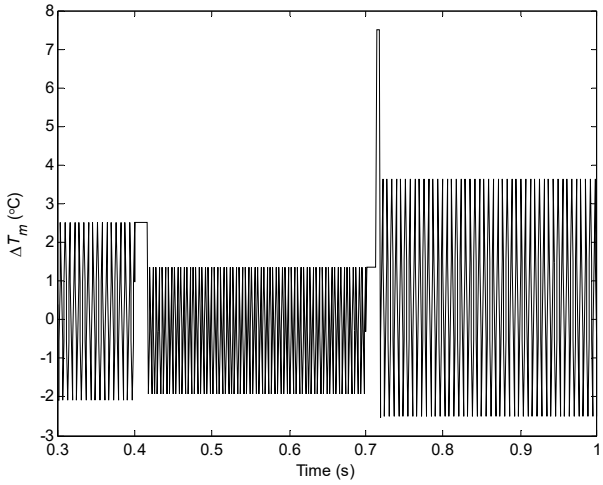

Figure 17. Curves under decreasing S conditions.

5.2.2. Simulation under Increasing Irradiance Conditions

By contrast, the second simulation is done under increasing irradiance conditions. Here, assuming that the irradiance changes in Figure 18. The simulation results can be shown in Figures 19–23. In this case, the controller must operate at the "Increasing S mode" twice.

Figures 19 and 20 show that when the estimation method is used, S_m and I_m can be calculated by Equation (8) under increasing irradiance conditions. Here, their mean values are approximately accurate, although there are also some ripples. Figure 21 shows that S_I can be successfully calculated by Equation (10) when the irradiance keeps increasing. Figure 22 shows that, firstly, S_m has a very small error under increasing irradiance conditions. Secondly, there is a small error for S_I. Thirdly, when there is a sudden change in the irradiance, their errors exist in the peak values because of the inertia and delay of the whole PV system. Figure 23 shows that, on the one hand, the mean values of T_m have a small error under increasing conditions. On the other hand, there exists some oscillation for these errors because of the inertia and delay of the PV system, especially at the time of the sudden change of the irradiance.

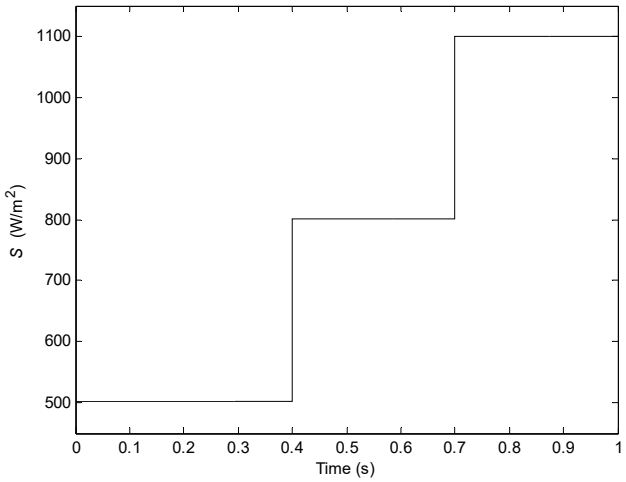

Figure 18. Assumed irradiance curve in second simulation.

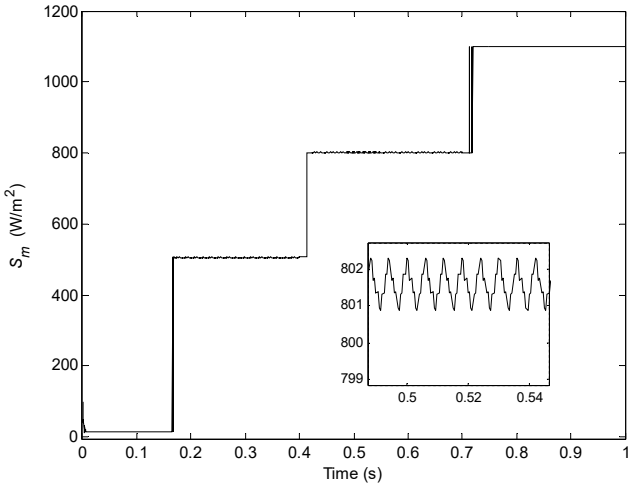

Figure 19. Curve in second simulation.

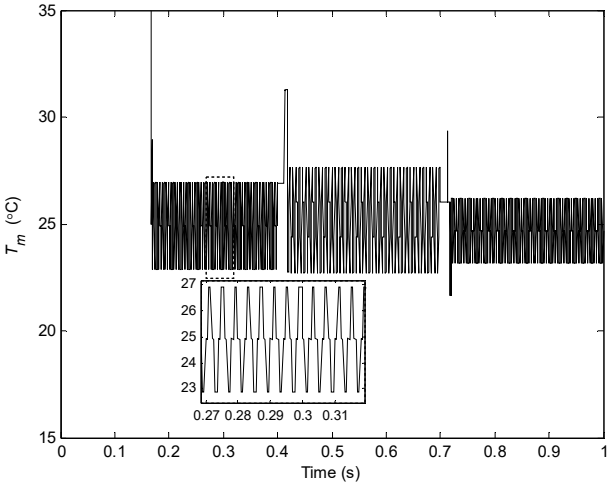

Figure 20. Curve in second simulation.

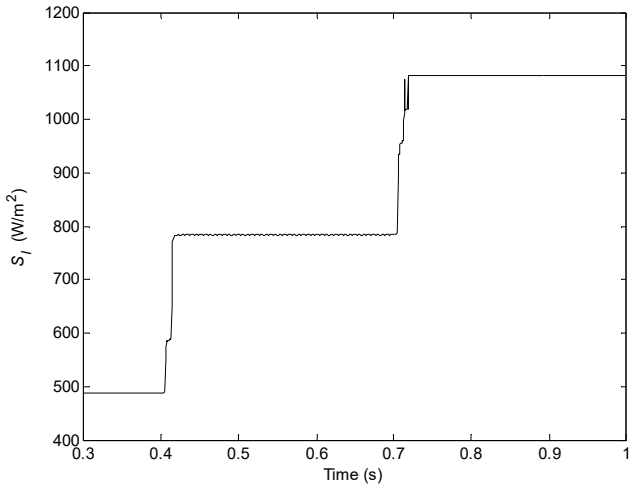

Figure 21. Curve in second simulation.

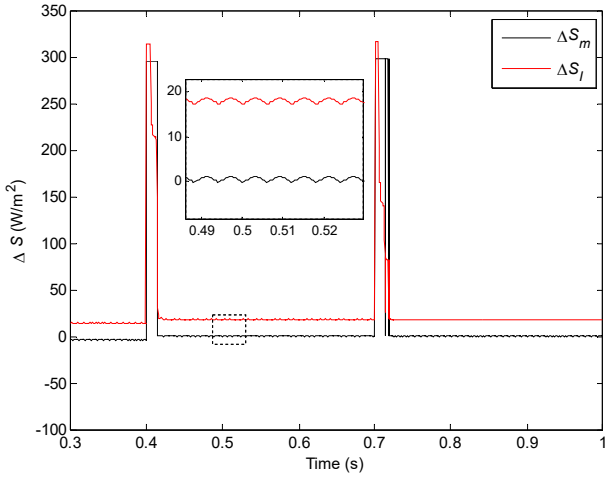

Figure 22. ΔS_I curves under increasing S conditions.

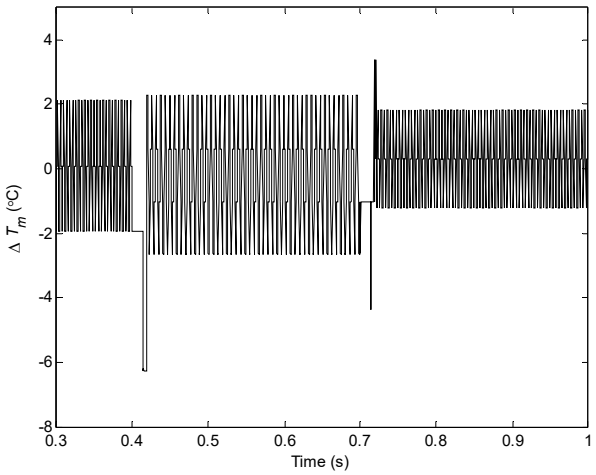

Figure 23. ΔT_m curve under increasing S conditions.

In a word, under varying weather conditions, the estimation method is feasible, available, and workable to obtain the real-time I&T values, and its accuracy is very good regardless of the increasing or decreasing irradiance conditions.

5.3. Feasibility, Availability, and Accuracy of the VWPOS

5.3.1. Accuracy of the Main Control Variables

For the proposed VWPOS, two simulation experiments are performed to analyze its control process and test its feasibility, availability, and accuracy. The weather conditions of these two simulations are the same as in Section 5.2. Simulation results are shown in Figures 24–29. In these simulations, the P&O method is used as the optimized object because of its extensive use, easy implementation, and low cost. Assuming that the VWPOS starts operating at 0.3 s and the MPP is tracked only by the P&O method before 0.3 s. Here, ΔV_m and ΔD_m are defined by Equation (22) and Equation (23), respectively. In Figure 28, ΔV_{mI} and ΔV_{mD} represent the ΔV_m corresponding to the increasing and decreasing irradiance conditions, respectively. Meanwhile, in Figure 29, ΔD_{mI} and ΔD_{mD} represent the ΔD_m corresponding to the increasing and decreasing irradiance conditions, respectively. In Equation (23), $D_{\max}$ represents the ideal value of D at the MPP.

$$\Delta V_m = V_{PV} - C \tag{22}$$

$$\Delta D_m = D - D_{\max} \tag{23}$$

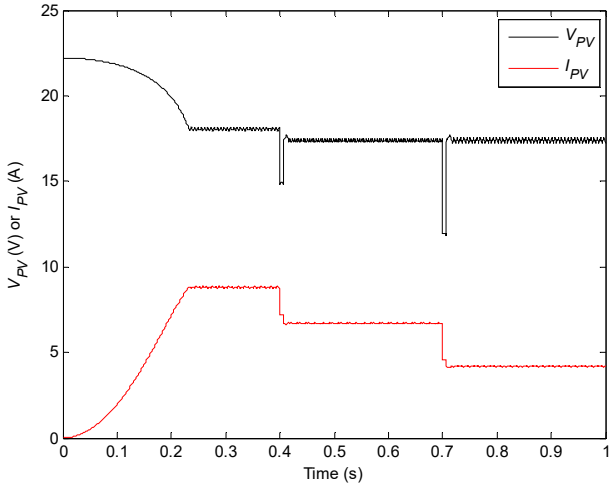

Figure 24. I_{PV} curves in first simulation.

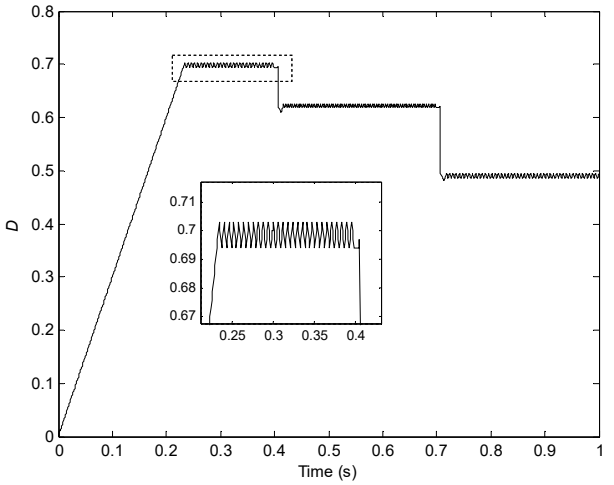

Figure 25. Duty cycle curve in first simulation.

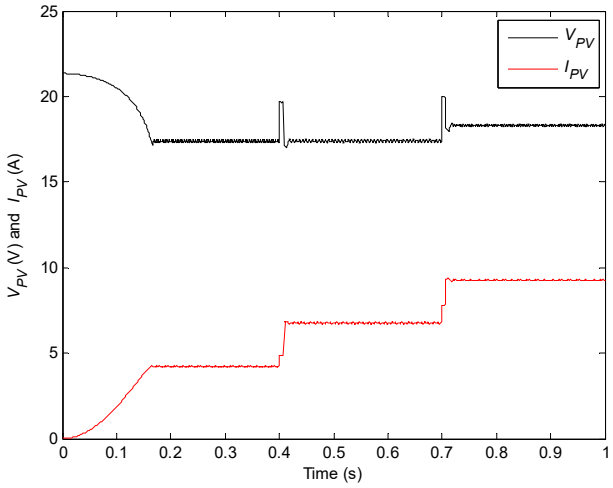

Figure 26. V_{PV} and I_{PV} curves in second simulation.

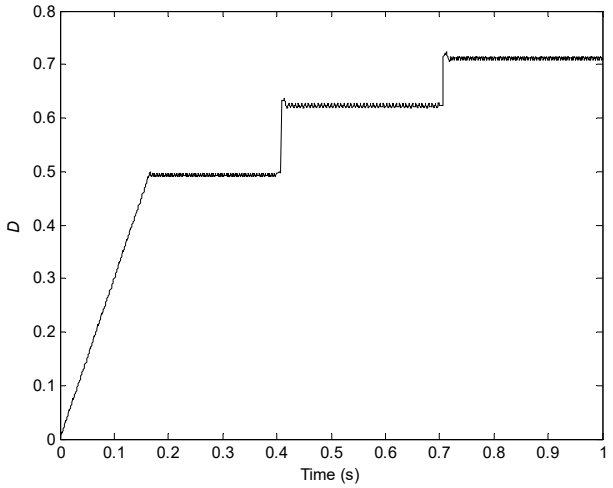

Figure 27. Duty cycle curve in second simulation.

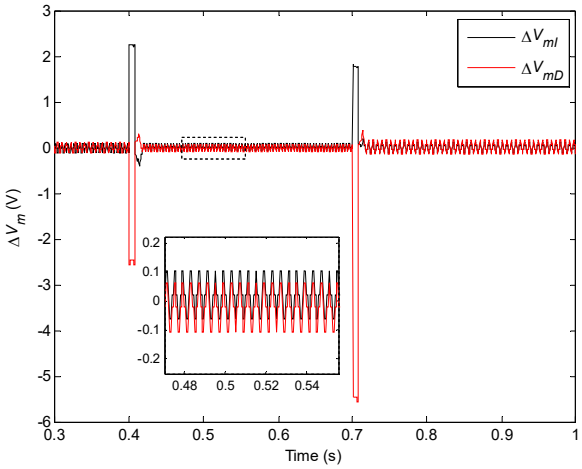

Figure 28. Curves under two conditions.

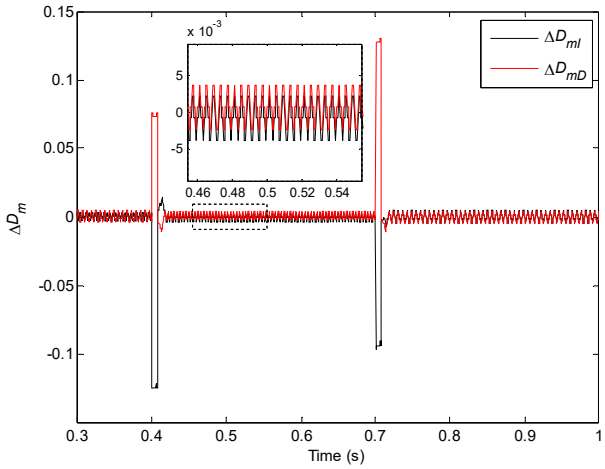

Figure 29. Curves under two conditions.

Figures 24 and 25 show that, under decreasing irradiance conditions, on the one hand, before the VWPOS is used, the MPP is searched only by the P&O method. The tracking speed can not be improved. On the other hand, after the VWPOS is used, the MPP is tracked by the optimized P&O method. In this case, the MPPT speed is greatly improved. Figures 26 and 27 show that, under increasing irradiance conditions, on the one hand, before the VWPOS is used, the MPP is searched only by the P&O method. The tracking speed can not be improved. On the other hand, after the VWPOS is used, the MPP is tracked by the optimized P&O method. In this case, the MPPT speed is greatly improved.

Figure 28 shows that the error between V_{PV} and C is always less than 0.1 V regardless of the increasing or decreasing irradiance conditions, while there exists some oscillation at the time of the sudden change of the irradiance. Figure 29 shows that the error between D and its ideal value at the MPP ($D_{\max}$) is always less than 0.005 regardless of the increasing or decreasing irradiance conditions, while there exists some oscillation at the time of the sudden change of the irradiance.

Clearly, these results show that the PV system using the VWPOS can work well along the control flow shown in Figure 11 regardless of the increasing irradiance or decreasing irradiance conditions. Meanwhile, these results also show that the MPPT rapidity can be greatly improved by using the VWPOS. Therefore, a conclusion can be drawn that the VWPOS is feasible, workable, and accurate.

5.3.2. Analysis of the Control Signal and Output Power

To further test the feasibility, availability, and accuracy of the VWPOS, some simulations are conducted under arbitrary irradiance conditions. Here, for the solar irradiance, assuming that there are some step changes whose initial values and final values are given in Table 8. The simulation results of the VWPOS and P&O methods are given in Table 8. Meanwhile, the ideal control signals ($D_{\max}$) and ideal output powers ($P_{o\max}$) at the MPP are also shown to make a comparison.

Table 8 shows that, firstly, both $D_{\max P}$ and $D_{\max \&}$ are always approximately equal to $D_{\max}$. Meanwhile, $P_{o\max P}$ is always approximately equal to $P_{o\max \&}$. Secondly, the average error between $D_{\max}$ and $D_{\max P}$ is 0.00005. It is far less than the average error between $D_{\max}$ and $D_{\max \&}$ (0.00025). Thirdly, the average error between $P_{o\max}$ and $P_{o\max P}$ (2.863 W) is less than the average error between $P_{o\max}$ and $P_{o\max \&}$ (2.864 W). Clearly, by using the VWPOS, on the one hand, the MPP can be reached successfully. On the other hand, the control signals are more accurate than the P&O method, while their output powers are approximately equal.

In a word, the VWPOS is feasible and available to reach the MPP successfully, and there is a good accuracy.

Table 8. Simulation results under arbitrary irradiance conditions.

Initial Values (W/m^2)	Final Values (W/m^2)	D_{max}	D_{maxP}	$D_{max\&}$	P_{omax} (W)	P_{omaxP} (W)	$P_{omax\&}$ (W)
300	500	0.4919	0.4920	0.4915	73.083	70.767	70.755
300	1100	0.7113	0.7121	0.7120	169.171	165.638	165.647
500	800	0.6216	0.6209	0.6220	117.163	114.228	114.233
500	1100	0.7113	0.7104	0.7120	169.171	165.650	165.648
700	400	0.4377	0.4375	0.4376	59.069	56.985	56.977
700	900	0.6556	0.6555	0.6550	133.332	130.205	130.204
700	1100	0.7113	0.7118	0.7120	169.171	165.649	165.647
900	500	0.4919	0.4913	0.4915	73.083	70.764	70.755
900	600	0.5402	0.5423	0.5410	87.273	84.742	84.739
900	1100	0.7113	0.7108	0.7120	169.171	165.639	165.646
1000	800	0.6216	0.6210	0.6220	117.163	114.222	114.230
1000	600	0.5402	0.5400	0.5410	87.273	84.732	84.740
1000	500	0.4919	0.4918	0.4915	73.083	70.765	70.755

5.4. MPPT Optimization Effect of the VWPOS

5.4.1. Influence of the Different Tracking Step Sizes

In order to analyze the influence of the different tracking step sizes on the optimization effect of the VWPOS, a simulation experiment is performed under 30 °C and 1.5 Ω conditions. Here, assuming that the solar irradiance keeps varying with Figure 30 and the VWPOS starts working at 4.5 s (its step "Initialization" is before 4.5 s). Meanwhile, the selected step sizes of the P&O method optimized by the VWPOS are 0.002 and 0.003. They are represented by "Proposed strategy with 0.002" and "Proposed strategy with 0.003", respectively. Finally, Figures 31 and 32 and Table 9 show the results. In addition, the conventional P&O method is compared with the VWPOS, and it is represented by "P&O method with 0.003" in Figures 31 and 32.

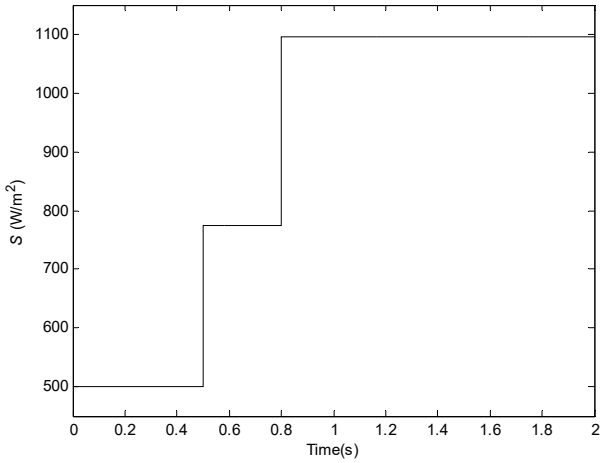

Figure 30. Curve under different step size conditions.

Figures 31 and 32 show that, after the VWPOS works, the MPP can always be reached successfully. Meanwhile, according to Figures 31 and 32, and Table 9, it can be seen that, firstly, the steady-state accuracy and oscillation can be improved by the decrease in the tracking step size to a certain extent. Secondly, when the VWPOS is used, the MPPT speed is hardly influenced by the decrease in the tracking step size. Thirdly, the tracking speed of the conventional P&O method can be greatly increased by the use of the VWPOS.

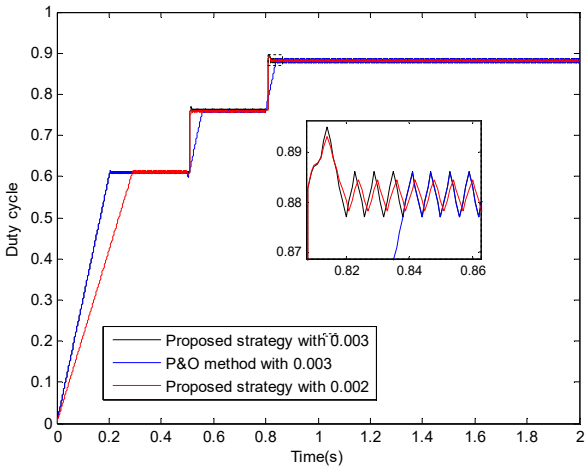

Figure 31. Duty cycle curves under different step size conditions.

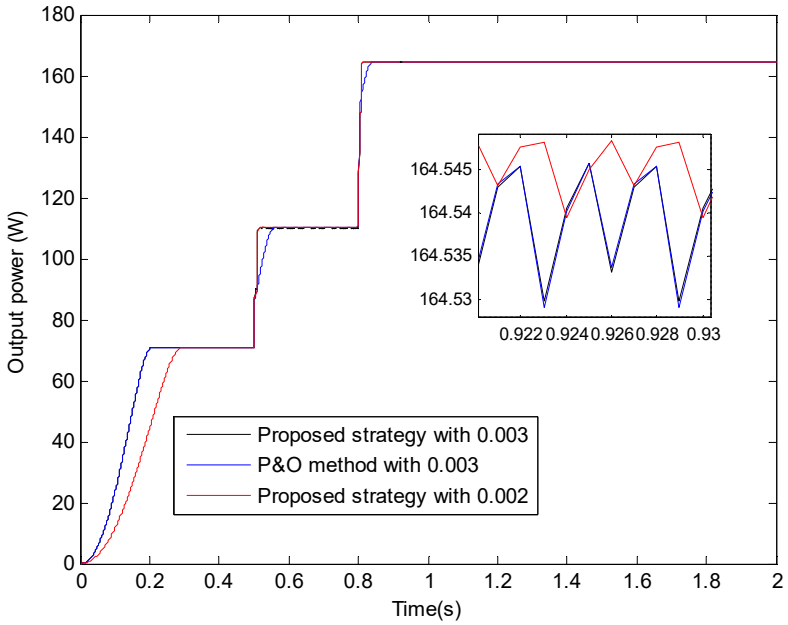

Figure 32. Compared power curves under different step size conditions.

Table 9. Simulation parameters and results corresponding to Figures 30–32.

Range of Time (s)	S (W/m^2)	$D_{\max}$	$P_{o\max}$ (W)	$D_{\max P1}$	$D_{\max P2}$	$D_{\max\&}$	$P_{o\max 1}$ (W)	$P_{o\max 2}$ (W)	$P_{o\max\&}$ (W)	t_s^1 (ms)	t_s^2 (ms)	$t_s^\&$ (ms)
[0, 0.5]	500	0.6106	72.931	0.609	0.611	0.609	70.619	70.621	70.619	/	/	204
[0.5, 0.8]	774	0.7598	112.878	0.760	0.760	0.760	110.004	110.005	110.004	14	14	56
[0.8, 2]	1096	0.8818	168.051	0.882	0.882	0.882	164.539	164.545	164.539	13	13	40

5.4.2. Comparison with Other MPPT Methods

In order to assess the MPPT performance of the VWPOS, a simulation experiment is also performed under 30 °C and 1.5 Ω conditions. Here, assuming that the solar irradiance keeps varying with Figure 33 and the VWPOS starts working at 4.5 s (its step "Initialization" is before 4.5 s). Meanwhile, the conventional P&O method and VWP method 1 in Ref. [5] are selected as the compared objects. Finally, Figures 34 and 35 and Table 10 show the results.

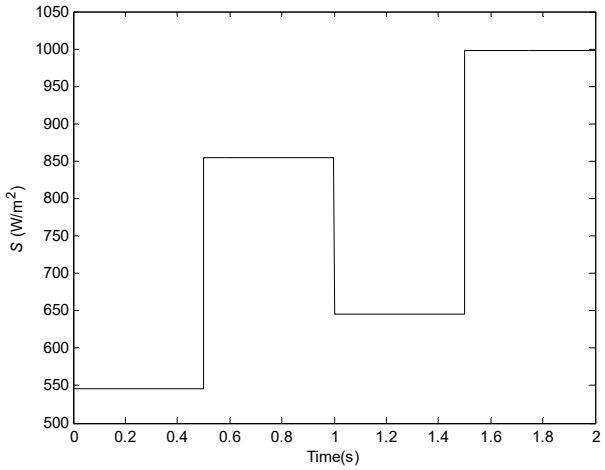

Figure 33. Irradiance curve for the comparison experiment.

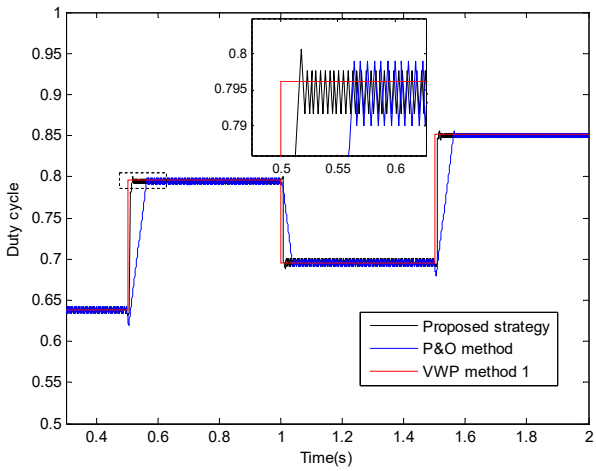

Figure 34. Compared duty cycle curves of the different methods.

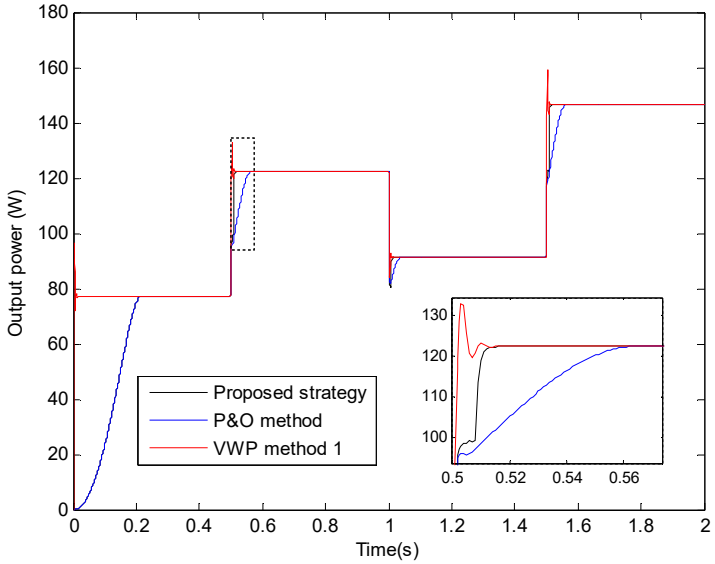

Figure 35. Compared power curves of the different methods.

Table 10. Simulation parameters and results corresponding to Figures 33–35.

Range of Time (s)	S (W/m^2)	$D_{\max}$	$P_{o\max}$ (W)	$D_{\max P1}$	$D_{\max \&}$	$D_{\max V}$	$P_{o\max P1}$ (W)	$P_{o\max \&}$ (W)	$P_{o\max V}$ (W)	t_s^1 (ms)	$t_s^{\&}$ (ms)	t_s^V (ms)
[0.3, 0.5]	546	0.6391	79.408	0.6380	0.6380	0.6375	76.991	76.991	76.999	/	214	18
[0.5, 1]	854	0.7951	125.508	0.7940	0.7940	0.7962	122.477	122.474	122.481	16.5	64	14
[1, 1.5]	646	0.6959	93.732	0.6950	0.6950	0.6953	91.108	91.105	91.118	12	37	17
[1.5, 2]	998	0.8501	149.935	0.8502	0.8502	0.8514	146.622	146.623	146.627	14	62	16

Figures 34 and 35 show that, after the VWPOS works, the MPP can always be reached successfully by three MPPT methods. Meanwhile, according to Figures 34 and 35, and Table 10, it can be seen that, firstly, when the PV systems with three MPPT methods operate at their own MPPs, the duty cycles and output powers are nearly equal. Secondly, the setting time of the VWPOS is the best, while there is the fastest response speed for the VWP method 1. Thirdly, the VWPOS and conventional P&O methods have no overshoot. Fourthly, when the conventional P&O method with the steady-state oscillation is selected as the optimized object, this oscillation still exists even if the VWPOS is used. Finally, the VWPOS has a lower cost than VWP method 1 because the I&T sensors are saved.

In a word, by using the VWPOS, the MPPT speed can be greatly improved, and the smaller seeking step size with the same tracking speed can be implemented to obtain better steady-state accuracy and oscillation.

6. Discussions

In this work, two main limitations of this strategy maybe exist. On the one hand, two key expressions (Equations (10) and (11)) have been built when the cell parameters I_{sc}, V_{oc}, I_m and V_m are selected as 9.19 A, 22 V, 8.58 A and 17.5 V, respectively. This limitation may cause a lot of inconvenience in using this proposed strategy. However, in practical application, the equations to match the different PV cells can be found easily, and a corresponding list for the user can be built. On the other hand, these expressions are presented on the basis of the buck DC/DC converter. However, in practical application, the results on other DC/DC converters can also be obtained easily by analogy.

Meanwhile, there are some given assumptions in the simulation experiments. However, the final conclusions on this strategy are hardly influenced by them. On the one hand, the assumed operating conditions are usually some step signals. It is well known that these signals are the most severe in practical application. On the other hand, although some operating conditions are selected in this work, others can be analyzed by analogy. In addition, because the P&O method can be regarded as the representation of the existing MPPT methods and has been widely used in practical applications, in this paper, it is selected as the optimized object. However, other MPPT methods can also be analyzed by analogy.

As to the error estimation of this strategy, two aspects can be illustrated as follows: on the one hand, because the MPP is tracked by a selected MPPT method within γ_2, the MPPT error is determined by this method. According to Tables 8–10, the error is so small that it can be ignored when the PV system has arrived at the MPP. On the other hand, there exists some error arising from Equations (8) and (10)–(13). According to the results in Figures 16, 17, 22 and 23, the absolute values of ΔS_m, ΔS_D, ΔS_I and ΔT_m are less than 5 W/m^2, 15 W/m^2, 20 W/m^2, and 0.5 °C. However, the accuracy of the control signal is hardly influenced by them. A piece of evidence is that, according to Figure 29, ΔD_{mI} and ΔD_{mD} are always less than 0.005. Therefore, the error can be ignored because the aim of using them is to obtain the region γ_2.

The existing MPPT methods or strategies are usually classified as classical methods, intelligent methods, and other methods. The P&O method can be regarded as the representative of the classical methods, the FLC method can be regarded as the representative of the intelligent methods, and the VWP method is selected as the representative of other

methods. Table 11 shows the main advantages and disadvantages of these methods to make a comparison of VWPOS with other MPPT methods. It can be seen from Table 11 that some advantages originating from the VWP methods have been inherited, while its MPPT speed is sacrificed to a certain extent to reduce the hardware cost via the abandonment of the I&T sensors.

Table 11. Comparison VWPOS with other MPPT methods.

MPPT Methods or Strategies	Main Advantages	Main Disadvantages
VWPOS	(1) faster MPPT speed; (2) no requirement for I&T sensors or external I&T data.	(1) slower MPPT speed than VWP method 1; (2) steady-state performance determined by its optimization object (existing MPPT methods).
P&O method	(1) easy implementation; (2) low requirements for microprocessor; (3) low hardware cost.	(1) slowest MPPT speed; (2) steady-state oscillation.
FLC method	(1) fast MPPT speed; (2) scarcely any steady-state oscillation.	(1) slower MPPT speed than VWP method 1 or VWPOS; (2) higher hardware cost (including microprocessor).
VWP method 1	(1) fastest MPPT speed; (2) no steady-state oscillation.	(1) overshoot; (2) requirements for I&T sensors or external I&T data.

7. Conclusions

In this work, an estimation method for obtaining the real-time irradiance or temperature value has been attempted. It includes two aspects: on the one hand, an established equation set is solved to obtain the real-time I&T values under changeless weather conditions. On the other hand, two empirical equations are discovered to calculate the real-time irradiance value under varying weather conditions. Based on these estimated I&T values, a VWP MPPT optimization strategy is proposed. Comparing it with VWP methods, the main advantage is the inheritance of the MPPT rapidity without irradiance and temperature sensors. Finally, many simulations verify the feasibility, availability, and workability of the estimation method and proposed optimization strategy. This work can solve the cost problem arising from irradiance and temperature sensors for all VWP methods, which is greatly beneficial for their practical application.

Future work on the subject will be focused on applying this proposed optimization strategy to optimize other existing MPPT methods. Here, the computational speed of the control program should be one of the research emphases when the PV system is operating under fast varying weather conditions.

Funding: This work was supported by National Natural Science Foundation of China (No. 61963014) and High-level Achievement Cultivation Project of Hubei Minzu University (No. PY21004).

Acknowledgments: The author would like to sincerely thank the editor and anonymous reviewers for their valuable comments and suggestions to improve the quality of the article.

Conflicts of Interest: The author declares no conflict of interest.

Abbreviations

MPPT	maximum power point tracking
VWP	variable-weather-parameter
MPP	maximum power point
PV	photovoltaic
PWM	pulse-width modulation
STC	standard test conditions
P&O	perturbation and observation
FLC	fuzzy logic control
PSO	particle swarm optimization
INC	incremental conduction
VWPOS	VWP optimization strategy
I&T	irradiance and temperature

Nomenclature

I_{sc}	short circuit current at STC (A)
I_m	MPP current at STC (A)
V_{oc}	open circuit voltage at STC (V)
V_m	MPP voltage at STC (V)
V_{PV}	output voltage of PV cell (V)
I_{PV}	output current of PV cell (A)
S	solar irradiance (W/m^2)
T	cell temperature (°C)
R_L	load resistance (Ω)
P_o	output power of PV system (W)
D	duty cycle of the PWM signal of the DC/DC converter
C	V_{PV} corresponding to the MPP of PV system (V)
$P_{o\mathrm{max}}$	ideal or calculated value of the maximum output power (W)
$P_{o\mathrm{maxP}}$	maximum output power using the proposed strategy (W)
$P_{o\mathrm{max\&}}$	maximum output power using the P&O method with 0.003 step size (W)
$P_{o\mathrm{maxP1}}$	$P_{o\mathrm{maxP}}$ when the step size of the optimized P&O method is 0.003 (W)
$P_{o\mathrm{maxP2}}$	$P_{o\mathrm{maxP}}$ when the step size of the optimized P&O method is 0.002 (W)
$P_{o\mathrm{maxV}}$	maximum output power using the VWP method 1 in Ref. [5] (W)
D_{max}	ideal or calculated value of the duty cycle at the MPP
D_{maxP}	duty cycle at the MPP using the proposed strategy
$D_{\mathrm{max\&}}$	duty cycle at the MPP using the P&O method
D_{maxP1}	D_{maxP} corresponding to $P_{o\mathrm{maxP1}}$
D_{maxP2}	D_{maxP} corresponding to $P_{o\mathrm{maxP2}}$
D_{maxV}	duty cycle at the MPP using the VWP method 1 in Ref. [5]
t_s^1	settling time corresponding to $P_{o\mathrm{maxP1}}$ (ms)
t_s^2	settling time corresponding to $P_{o\mathrm{maxP2}}$ (ms)
$t_s^{\&}$	settling time corresponding to $P_{o\mathrm{max\&}}$ (ms)
t_s^{V}	settling time corresponding to $P_{o\mathrm{maxV}}$ (ms)

References

1. Belkaid, A.; Colak, I.; Isik, O. Photovoltaic maximum power point tracking under fast varying of solar radiation. *Appl. Energy* **2016**, *179*, 523–530. [CrossRef]
2. Danandeh, M.A.; Mousavi, G.S.M. Comparative and comprehensive review of maximum power point tracking methods for PV cells. *Renew. Sustain. Energy Rev.* **2018**, *82*, 2743–2767. [CrossRef]
3. Li, X.; Wen, H.; Hu, Y.; Jiang, L. A novel beta parameter based fuzzy-logic controller for photovoltaic MPPT application. *Renew. Energy* **2019**, *130*, 416–427. [CrossRef]
4. Hong, Y.-Y.; Beltran, A.A., Jr.; Paglinawan, A.C. A robust design of maximum power point tracking using Taguchi method for stand-alone PV system. *Appl. Energy* **2018**, *211*, 50–63. [CrossRef]
5. Gao, X.; Li, S.; Gong, R. Maximum power point tracking control strategies with variable weather parameters for photovoltaic generation systems. *Sol. Energy* **2013**, *93*, 357–367. [CrossRef]
6. Li, S. A maximum power point tracking method with variable weather parameters based on input resistance for photovoltaic system. *Energy Convers. Manag.* **2015**, *106*, 290–299. [CrossRef]

7. Li, S. A variable-weather-parameter MPPT control strategy based on MPPT constraint conditions of PV system with inverter. *Energy Convers. Manag.* **2019**, *197*, 111873. [CrossRef]
8. Sher, H.A.; Murtaza, A.F.; Noman, A.; Addoweesh, K.E.; Al-Haddad, K.; Chiaberge, M. A new sensorless hybrid MPPT algorithm based on fractional short-circuit current measurement and P&O MPPT. *IEEE Trans. Sustain. Energy* **2015**, *6*, 1426–1434.
9. Li, S. A MPPT speed optimization strategy for photovoltaic system using VWP interval based on weather forecast. *Optik* **2019**, *192*, 162958. [CrossRef]
10. Guo, S.; Abbassi, R.; Jerbi, H.; Rezvani, A.; Suzukie, K. Efficient maximum power point tracking for a photovoltaic using hybrid shufflfled frog-leaping and pattern search algorithm under changing environmental conditions. *J. Clean. Prod.* **2021**, *297*, 126573. [CrossRef]
11. Yang, B.; Yu, T.; Shu, H.; Zhu, D.; An, N.; Sang, Y.; Jiang, L. Perturbation observer based fractional-order sliding-mode controller for MPPT of grid-connected PV inverters: Design and real-time implementation. *Control Eng. Pract.* **2018**, *79*, 105–125. [CrossRef]
12. Veerapen, S.; Wen, H.; Li, X.; Du, Y.; Yang, Y.; Wang, Y.; Xiao, W. A novel global maximum power point tracking algorithm for photovoltaic system with variable perturbation frequency and zero oscillation. *Sol. Energy* **2019**, *181*, 345–356. [CrossRef]
13. Bahrami, M.; Gavagsaz-Ghoachani, R.; Zandi, M.; Phattanasak, M.; Maranzanaa, G.; Nahid-Mobarakeh, B.; Pierfederici, S.; Meibody-Tabar, F. Hybrid maximum power point tracking algorithm with improved dynamic performance. *Renew. Energy* **2019**, *130*, 982–991. [CrossRef]
14. Dehghani, M.; Taghipour, M.; Gharehpetian, G.B.; Abedi, M. Optimized fuzzy controller for MPPT of grid-connected PV systems in rapidly changing atmospheric conditions. *J. Mod. Power Syst. Clean Energy* **2021**, *9*, 376–383. [CrossRef]
15. Zhang, X.; Gamage, D.; Wang, B.; Ukil, A. Hybrid maximum power point tracking method based on iterative learning control and perturb & observe method. *IEEE Trans. Sustain. Energy* **2021**, *12*, 659–670.
16. Rezk, H.; AL-Oran, M.; Gomaa, M.R.; Tolba, M.A.; Fathy, A.; Ali Abdelkareem, M.; Olabi, A.G.; El-Sayed, A.H.M. A novel statistical performance evaluation of most modern optimization based global MPPT techniques for partially shaded PV system. *Renew. Sustain. Energy Rev.* **2019**, *115*, 109372. [CrossRef]
17. Lasheen, M.; Abdel-Salam, M. Maximum power point tracking using hill climbing and ANFIS techniques for PV applications: A review and a novel hybrid approach. *Energy Convers. Manag.* **2018**, *171*, 1002–1019. [CrossRef]
18. Cavalcanti, M.C.; Bradaschia, F.; do Nascimento, A.J., Jr.; Azevedo, G.M.S.; Barbosa, E.J. Hybrid maximum power point tracking technique for PV modules based on a double-diode model. *IEEE Trans. Ind. Electron.* **2021**, *68*, 8169–8181. [CrossRef]
19. Killi, M.; Samanta, S. Modified perturb and observe MPPT algorithm for drift avoidance in photovoltaic systems. *IEEE Trans. Ind. Electron.* **2015**, *62*, 5549–5559. [CrossRef]
20. Manoharan, P.; Subramaniam, U.; Babu, T.S.; Padmanaban, S.; Holm-Nielsen, J.B.; Mitolo, M.; Ravichandran, S. Improved perturb and observation maximum power point tracking technique for solar photovoltaic power generation systems. *IEEE Syst. J.* **2021**, *15*, 3024–3035. [CrossRef]
21. Mutoh, N.; Ohno, M.; Inoue, T. A method for MPPT control while searching for parameters corresponding to weather conditions for PV generation systems. *IEEE Trans. Ind. Electron.* **2006**, *53*, 1055–1065. [CrossRef]
22. Li, Q.; Zhao, S.; Wang, M.; Zou, Z.; Wang, B.; Chen, Q. An improved perturbation and observation maximum power point tracking algorithm based on a PV module four-parameter model for higher efficiency. *Appl. Energy* **2017**, *195*, 523–537. [CrossRef]
23. Gopi, R.; Sreejith, S. Converter topologies in photovoltaic applications—A review. *Renew. Sustain. Energy Rev.* **2018**, *94*, 1–14. [CrossRef]